JACC Vol. 7, No 4
April 1986:775–89

METHODS

Noninvasive Assessment of Coronary Stenoses by Myocardial Perfusion Imaging During Pharmacologic Coronary Vasodilation. VIII. Clinical Feasibility of Positron Cardiac Imaging Without a Cyclotron Using Generator-Produced Rubidium-82

K. LANCE GOULD, MD, FACC, RICHARD A. GOLDSTEIN, MD, FACC, NIZAR A. MULLANI, BS, RICHARD L. KIRKEEIDE, PHD, WAI-HOI WONG, PHD, TIMOTHY J. TEWSON, PHD, MARC S. BERRIDGE, PHD, LEONARD A. BOLOMEY, BS, ROSS K. HARTZ, MS, RICHARD W. SMALLING, MD, PHD, FACC, FRANCISCO FUENTES, MD, FACC, AKIRA NISHIKAWA, MD

Houston, Texas

The purpose of this study was to determine the clinical feasibility of diagnosing significant coronary artery disease by positron imaging of myocardial perfusion without a cyclotron, using generator-produced rubidium-82 (^{82}Rb). Fifty patients underwent positron emission tomography of the entire heart using a multislice positron camera and intravenous ^{82}Rb or nitrogen-13 ammonia ($^{13}NH_3$) before and after intravenous dipyridamole combined with handgrip stress. Images were read by two observers blinded as to clinical or arteriographic data.

Automated quantitative coronary arteriography was obtained for the arteriographic determination of coronary flow reserve, previously demonstrated to be a single integrated measure of stenosis severity accounting for all its geometric dimensions of length, absolute diameter, percent narrowing and asymmetry by quantitative analysis of cine films. Significant coronary artery disease was defined as an arteriographically determined coronary flow reserve of less than 3.0 based on all stenosis dimensions. Any single geometric measure of stenosis severity alone was an inadequate reference standard for comparison with perfusion images. Sensitivity of identifying patients with coronary artery disease having an arteriographically determined coronary flow reserve of less than 3.0 was 95% by positron imaging with a specificity of 100%. The single case that was missed, studied with $^{13}NH_3$, had a 43% diameter narrowing of a small ramus intermedius off the left coronary artery with no significant narrowing of the major coronary arteries.

Positron emission tomography of myocardial perfusion before and after intravenous dipyridamole combined with handgrip stress utilizing generator-produced ^{82}Rb provides sensitive and specific diagnosis of reduced coronary flow reserve due to coronary artery disease in humans.

(J Am Coll Cardiol 1986;7:775–89)

Coronary flow reserve has been previously validated by our laboratory (1) as a single measure of stenosis severity reflecting all its geometric dimensions of length, absolute diameter, percent narrowing and asymmetry. The concept of coronary flow reserve, first proposed by Gould et al. (2,3) in 1974, has been developed into a physiologic approach for identifying and quantifying the severity of coronary stenoses by noninvasive perfusion imaging based on three principles: optimization of a stimulus for maximizing coronary flow, an appropriate perfusion tracer and tomographic imaging (4–9). On the basis of these three steps, we have previously demonstrated (8,9) that cardiac positron emission tomography of cyclotron-produced nitrogen-13 ammonia ($^{13}NH_3$) injected intravenously during dipyridamole-induced coronary vasodilation is a promising nonin-

From the University of Texas Medical School, Division of Cardiology, the Positron Diagnostic and Research Center (PDRC) and the Graduate School of Biomedical Sciences, University of Texas Health Science Center at Houston, Houston, Texas. This work was carried out as a joint collaborative research project with the Clayton Foundation for Research and was supported in part by Grants R01HL26862 and R01HL26885 from the National Institutes of Health, Bethesda, Maryland and Grant DE-FG05-84ER60210 from the Department of Education, Washington, DC.

Manuscript received July 31, 1985; revised manuscript received October 30, 1985, accepted November 12, 1985.

Address for reprints: K. Lance Gould, MD, University of Texas Medical School at Houston, Division of Cardiology, Box 20708, Houston, Texas 77025.

0735-1097/86/$3.50

JACC Vol 7, No 4
April 1986:775–89

vasive approach for the diagnosis of coronary artery disease in animals and humans. Although an important conceptual step, this study was of restricted practical significance because of limitations in each of these three steps. The stress for increasing coronary flow using intravenous dipyridamole alone was suboptimal; the perfusion tracer, $^{13}NH_3$, required an on-site cyclotron for synthesis; and the positron camera was a first generation prototype with limited imaging capabilities. Finally, at that time the clinical coronary arteriograms were interpreted by visual estimation of stenosis severity (9), which is now widely recognized to be inadequate as a reference standard for comparison with perfusion images.

In the current report we describe major advances in each of the three essential steps for stress perfusion imaging and demonstrate the clinical feasibility of routine positron emission tomography for the noninvasive assessment of coronary artery disease without a cyclotron. For the current study, optimal coronary vasodilation was achieved using intravenous dipyridamole combined with handgrip stress (10). Because $^{13}NH_3$ has been previously described as a perfusion imaging agent (8,9), it was used for comparison purposes in approximately half of the patients. A more readily obtainable radionuclide, ^{82}Rb, from an ^{82}Sr-^{82}Rb generator, was injected intravenously as a perfusion indicator (11) at rest and during coronary vasodilation. Simultaneous multislice tomography of the entire heart was carried out using the University of Texas positron camera (12–17). Finally, clinical coronary arteriograms were quantitatively analyzed by an automated technique developed in our laboratory utilizing simultaneously both border recognition algorithms and integrated, arterial cross-sectional densitometry to obtain all geometric dimensions of the stenosis with an accuracy of ± 0.1 mm for diameters less than 0.5 mm (18,19) and a reproducibility of 2 to 3% (20,21). The program also predicts the pressure-flow characteristics (20,21) and coronary flow reserve of the stenosis (1) based on precise geometric dimensions as validated in vivo by direct flowmeter pressure measurements in instrumented dogs.

The results of blinded reading of images in 50 patients indicate that our protocol, consisting of intravenous dipyridamole, combined with handgrip stress and positron tomography of the entire heart using the University of Texas positron camera, has a 95% sensitivity and 100% specificity for identifying significant coronary artery disease as determined by automated quantitative arteriography. We describe the basic anatomy and principles for interpreting positron perfusion tomographs. The results also document the necessity of simultaneous multislice, contiguous tomographs of the entire heart with overlapping image planes. Single slice or multislice tomographic images without overlapping image planes, or with poorly sampled gaps between image planes, may lead to artifacts and erroneous interpretation due to image plane displacement on studies before and after pharmacologic stress. By eliminating the need for a cyclotron, demonstrating excellent sensitivity and specificity, establishing the principles of interpreting tomographic perfusion images and by reducing camera cost through dedicated, clinically oriented design, we have demonstrated that positron emission tomography of myocardial perfusion is clinically useful and economically feasible for accurate noninvasive assessment of coronary artery disease.

Methods

Patient selection and workup. Fifty patients were admitted to the protocol who were undergoing diagnostic cardiac catheterization for clinical indications of chest pain syndromes, electrocardiographic changes on exercise testing, evaluation after myocardial infarction, before and after percutaneous transfemoral coronary angioplasty or as part of a protocol of quantitative coronary arteriography before and after plasmaphoresis for cholesterol control. For all patients an admission history, physical examination, chest X-ray study, electrocardiogram and routine laboratory tests were performed. After informed consent for clinical study was obtained, coronary arteriography was performed by the transfemoral, percutaneous technique using Judkins preformed catheters passed through a sheath; less commonly the brachial artery approach with a Sones catheter was used. All patients were fully heparinized after the insertion of catheters. Multiple coronary arteriograms were obtained using 3 to 6 cc of Hypaque-76 per injection with a biplane Siemens 5–7–9 inch image intensifier; the X-ray tube was a Siemens Opti 150/40/72c with a 0.6 to 1.0 mm focal spot operating at 4 to 6 ms exposures, 300 mA s and 109 kV. Low contrast Vari-Cath cine film was used at 30 to 60 frames/s. Special effort was made to obtain orthogonal views for subsequent quantitative analysis. Resolution of the cine system is four to five line pairs per millimeter; pincushion distortion and variation of magnification in different parts of the field were less than 5% except at the corners of the field but were routinely corrected by a grid of known dimensions.

Analysis of coronary arteriograms. Cine X-ray frames were digitized on a Spatial Data System, Eyecom II on-line with a VAX 11/780 computer. Each stenosis of major proximal coronary arteries on orthogonal coronary arteriograms were analyzed as previously described (1,18,19) using both border recognition algorithms and arterial cross-sectional densitometry to determine stenosis dimensions, including integrated length for tapering stenoses, absolute cross-sectional area, relative percent narrowing and asymmetry of stenoses. The program is automated without operator intervention except to identify the stenotic region of the artery to be analyzed. From the stenosis dimensions, pressure-flow characteristics (20,21) and coronary flow reserve (1) were calculated automatically as previously validated. The au-

tomated analysis system is accurate to within ± 0.1 mm for contrast-filled phantoms with diameters of 0.5 mm or less in a scattering medium (18,19) and is reproducible to within 2 to 3% (20,21). The entire analysis routine requires 10 to 15 minutes per stenosis with a printout of all dimensions and functional measures of severity derived from stenosis geometry.

Radionuclides. *Rubidium-82* was eluted from an ^{82}Sr-^{82}Rb generator (11) using a 50 cc syringe driven by a microprocessor-controlled motor connected to an on-line radiation monitor that provided preset volume, dose and dose rate of ^{82}Rb to the patient. Typically, with a fresh generator, 30 to 50 mCi were injected in a 10 cc volume over 20 to 25 seconds. Toward the end of the useful life of the generator (6 weeks), volumes of 30 to 40 cc were required to deliver 30 to 50 mCi of ^{82}Rb. With a half-life of only 75 seconds, approximately one-half to two-thirds of this activity reaches the arterial circulation, with the balance decaying in transit through the infusion tubing, the venous system and lungs. Twenty-seven patients were studied with ^{82}Rb. The selection of ^{82}Rb or $^{13}NH_3$ was determined by availability of the generator because its useful life is 6 weeks and a fresh generator was not always immediately available for these developmental studies. When ^{82}Rb was unavailable, $^{13}NH_3$ was used.

Nitrogen-13 ammonia was produced using a 35 meV Scanditronix, positive ion, variable energy cyclotron. Our method utilizes the (p,α) reaction on oxygen-16 in water [$^{16}O(p,\alpha)\ ^{13}N$]. The water target was bombarded for 2 minutes with a proton beam of up to 40 μA at 17.2 meV. Production is typically 250 to 300 mCi of ^{13}N at the end of bombardment for a yield of 3 mCi/μA per min. The yield of ^{13}N is obtained largely in the form of nitrate. Next, 30 cc of bombarded water is transferred to a 50 cc flask equipped with a short path distillation head containing sodium hydroxide. Titanium trichloride is added to produce titanium (OH_3), a strong reducing agent that converts the nitrogen-13 nitrate to $^{13}NH_3$. The $^{13}NH_3$ is then recovered as approximately 40 mCi in 3 to 4 cc of distillate within 5 minutes. Fluorine-18 formed from the p,n reaction on oxygen-18, comprising on 2% of total activity, and other contaminants knocked out of the foil by the proton beam are removed by the distillation thereby providing a final product free of chemical and radionuclide contaminants. Ten to 20 mCi of $^{13}NH_3$ was injected intravenously and positron imaging was carried out as described in the following Imaging protocol section. Twenty-three patients were studied with $^{13}NH_3$.

Positron emission tomography. The University of Texas positron emission tomograph has been designed for whole body imaging. It has 720 cesium fluoride detectors (18 mm diameter × 45 mm long scintillators) arranged in five rings of 144 detectors each, to produce nine slices simultaneously. The geometric intrinsic resolution of the detectors has been measured at 8.1 mm full width half maximum (FWHM). The sensitivity of the camera, for a 20 cm diameter uniform source filled with 1 μCi/cc of radioactivity, has been measured at 7,000 coincidence counts/s per slice for the outer slices and in excess of 20,000 counts/s per slice for the inner five slices. The reconstructed resolution in an image is software controlled to be from 8 to 12 mm FWHM, depending on the statistical accuracy desired. The mechanical gantry has a slim (15 mm deep at the opening) spacious patient opening of 58 cm in diameter to allow ± 45° tilting of the gantry and ± 30° rotation of the bed relative to the gantry.

To provide the linear sampling required to reconstruct high resolution images, the detectors were made to "wobble" in a small circular motion of 19.6 mm in diameter. The wobble speed is variable but was set most commonly at once per second with a minimal scan time of 1 second. This wobble speed can be increased to two revolutions per second to improve the sampling during physiologic gating of the data collection with the heart cycle. The detectors can also move in the slice direction (Z direction) for a total of 20 mm to image more completely the space between the nine slices (10 mm separation between slices with a 15 mm slice thickness) to create a three-dimensional image of the distribution of radioactivity in the organ.

Processing of the images was achieved by a combination of a DEC Vax 11/750 computer and bit-slice microprocessors. Data can be collected either in the list mode for post-processing of images after the data collection or in the profile mode with the on-line microprocessors. The image mode creates backprojected images a few minutes after the data collection. Thus, the camera and its associated electronics have been designed for ease of patient management in a clinical environment.

Imaging protocol. After giving informed consent, the patient was brought to the positron imaging laboratory either before or after cardiac catheterization. Because the nine tomographic slices had to bracket the heart for optimal imaging, the patient was positioned in the tomograph according to a previously placed mark on the anterior chest corresponding to the lower border of the heart by fluoroscopy. Positioning the patient according to the point of maximal impulse on physical examination or by ultrasound was not sufficiently accurate in our experience. After positioning, transmission images were obtained using a gallium-68–filled plexiglass ring containing 3 mCi of gallium-68 ethylenediaminetetraacetic acid (EDTA) in a ring space 12 cm wide, 1 cm deep and 56 cm in diameter. After the transmission image, intravenous ^{82}Rb or $^{13}NH_3$ was then injected followed by data acquisition for 5 to 8 minutes for ^{82}Rb and 15 to 20 minutes for $^{13}NH_3$. Ten minutes after the administration of the first dose of ^{82}Rb, or 40 minutes for $^{13}NH_3$, dipyridamole was infused in a dose of 0.142 mg/kg per min for 4 minutes followed by flushing in the residual dipyridamole in the tubing at the end of 4 minutes. Two minutes later (sixth minute after the onset of dipyridamole infusion)

JACC Vol. 7, No 4
April 1986:775–89

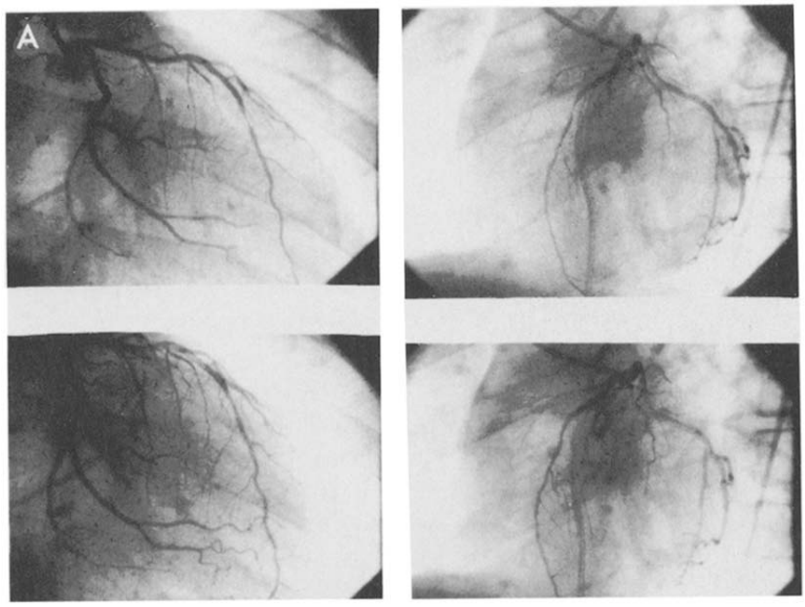

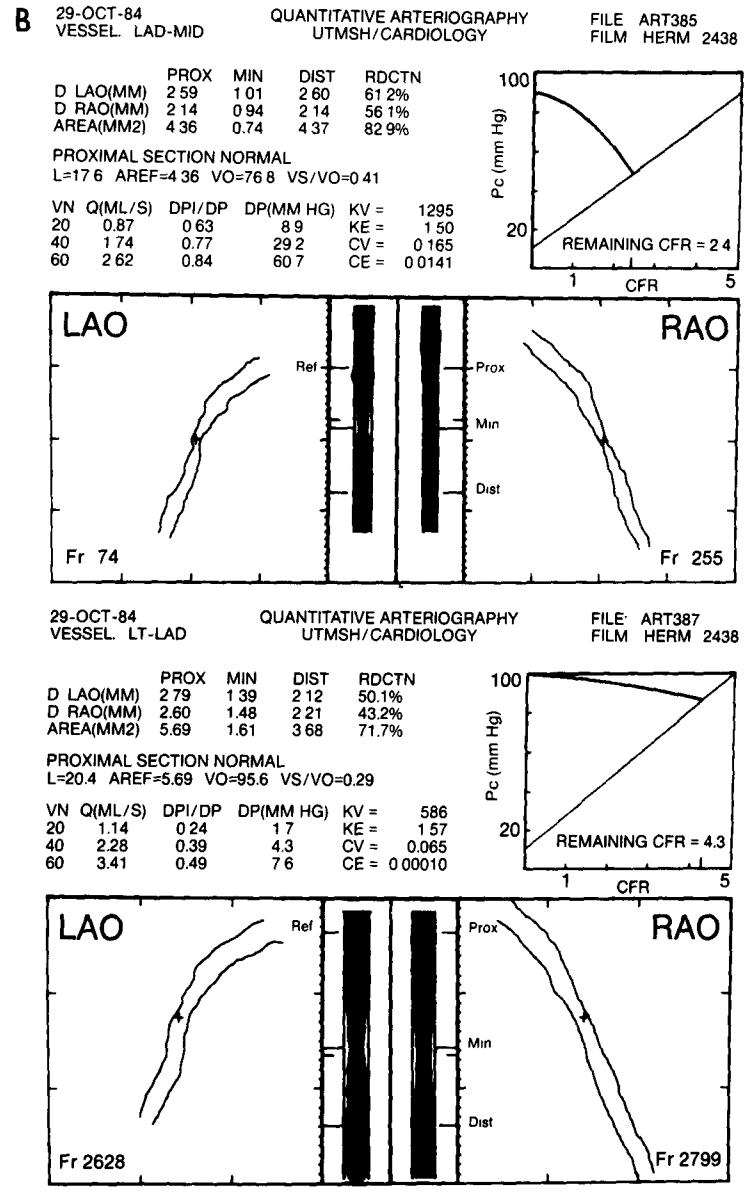

Figure 1. A, Coronary arteriogram in the left anterior oblique (**left**) and right anterior oblique (**right**) views before (**upper panels**) and after (**lower panels**) percutaneous transfemoral angioplasty. **B**, Computer printout of the quantitative arteriographic analysis before and after angioplasty. CFR = coronary flow reserve; D = diameter; DIST = distal artery; DP = pressure drop across stenosis in mm Hg: DPI/DP = proportion of pressure drop due to inertial and expansion (nonlinear) pressure loss; Fr = frame number; L = length in mm; LAO = left anterior oblique; MIN = minimal diameter; MM = millimeters; Pc = distal coronary pressure; PROX = proximal artery; Q = volume flow in ml/s; RAO = right anterior oblique; RDCTN = reduction in percent; VN = flow velocity in normal segment in cm/s.

unilateral handgrip at 25 to 30% of peak was begun by the patient on a hand dynamometer and held for 4 minutes. Four minutes after the end of the infusion of dipyridamole (and after 2 minutes of handgrip), ^{82}Rb or $^{13}NH_3$ was again injected with handgrip held for 2 more minutes. For patients who developed significant angina pectoris, aminophylline, 125 mg, was injected intravenously over 20 to 30 seconds. When angina pectoris occurred, it was always after the second infusion of ^{82}Rb had been completed. The same protocol was used for $^{13}NH_3$.

Transmission scans contained 80 to 100 million counts for all nine slices; emission images contained 10 to 14 million counts for ^{82}Rb (30 mCi dose) and 20 to 30 million counts for $^{13}NH_3$ (20 mCi dose) for nine slices. All nine slices were displayed simultaneously with optional magnification for any individual slice to examine details.

Twenty-seven patients were studied with ^{82}Rb and 23 were studied with $^{13}NH_3$. Of nine patients with normal arteriograms, five were studied with ^{82}Rb and four with $^{13}NH_3$. Of the 22 patients with an X-ray–determined coronary flow reserve of less than 3.0, 12 were studied with ^{82}Rb and 10 with $^{13}NH_3$. Of 13 patients with an X-ray–determined coronary flow reserve of 3.0 or greater, 7 were studied with ^{82}Rb and 6 with $^{13}NH_3$. The use of ^{82}Rb or $^{13}NH_3$ was determined solely by availability of the ^{82}Rb generator. When available, ^{82}Rb was always used; when ^{82}Rb was unavailable, $^{13}NH_3$ was used. Images with $^{13}NH_3$ provided a previously described reference for comparison with ^{82}Rb.

Image interpretation. All images were coded by number and interpreted visually by two observers blinded as to name, clinical status and findings on coronary arteriography. All images were read blindly three times in a procedure in which each reading session of all studies utilized one of three different presentation formats. The first presentation format, referred to here as the gray scale format, utilized a gray, black and white scale for count density with 20 to 30% background subtraction and comparison of rest-stress images on a slice by slice basis; that is, slice one at rest was compared with slice one at stress, slice two at rest compared with slice two at stress, and so forth, for each study.

The second format, termed the tricolor format, utilized a single color for transmission (red), rest (blue) and stress (green) images where color intensity indicated count density. All three images for each slice were superimposed. For a normal image, the superimposition of the red transmission, the blue rest and the green stress images produced a white tomogram of the heart muscle situated in a red transmission image of the thorax. With a stress defect, the relative contribution of the green color was diminished, leaving the rest blue color superimposed on the red transmission image. Consequently, stress defects not present at rest appeared as a purple color within white areas of normally perfused myocardium, thereby accentuating defects. A permanent defect or scar showed as an absence of both blue rest and green stress colors leaving the red transmission images showing through. Therefore, with this format, a defect at rest that persisted during stress appeared as a red area within normal white myocardium.

The third presentation scheme was termed the isocount color format. For this presentation, the range of count densities within all nine slices was scaled in 33 steps, each of which corresponded to 3% of maximal counts ranging in color from black for lowest counts (<20% of maximum), to blue (20 to 35% of maximum), to green (35 to 50% of maximum), to yellow (50 to 68% of maximum), to red (68 to 85% of maximum), to white (85 to 100% of maximal counts), with white being maximal counts. Within each of the five basic colors, there were approximately five hues of color gradations reflecting count density in steps 3% of maximal counts. In this scheme a defect appeared as a different color, blue or green, surrounded by yellow, red or white; however, there was a gradation in colors reflecting a continuum of changing count densities. For this presentation, the composite presentation of all nine slices was interpreted in toto for the entire heart on the rest and then stress studies. Slice by slice comparisons were *not* relied on because of the problem of translation of the heart along its long axis, or occasionally laterally, thereby causing a change in image planes or slice displacement between rest-stress studies. The entire series of patient studies was read in toto by each presentation scheme separately, separated by 1 to 2 weeks, all blinded as to name, diagnosis, clinical status and arteriographic data.

Results

Coronary arteriography. Fifty patients were studied. Twenty-two had coronary artery disease with an arteriographically determined coronary flow reserve of less than 3.0 by quantitative analysis of X-ray dimensions of the stenoses. Nine were without coronary artery disease. Thirteen had coronary artery disease with arteriographically determined coronary flow reserve of 3.0 or greater. Six patients were excluded from interpretation before tabulating results because of technical problems with the data. Because this series includes the first patient ever studied on the protocol, several mistakes were made initially in positioning patients. Of the six excluded patients, five were excluded because the tomographic field was too high and the bottom half of the heart was missed when positioning according to the palpable maximal impulse on physical examination. For that reason, we then marked the lower border of the heart by fluoroscopy to bracket the entire heart within the imaging field. One of the six patients was excluded because the attenuation data were lost as a consequence of a computer breakdown. For the 22 patients with significant coronary disease (coronary flow reserve <3.0), there were 18 left

JACC Vol 7, No. 4
April 1986:775–89

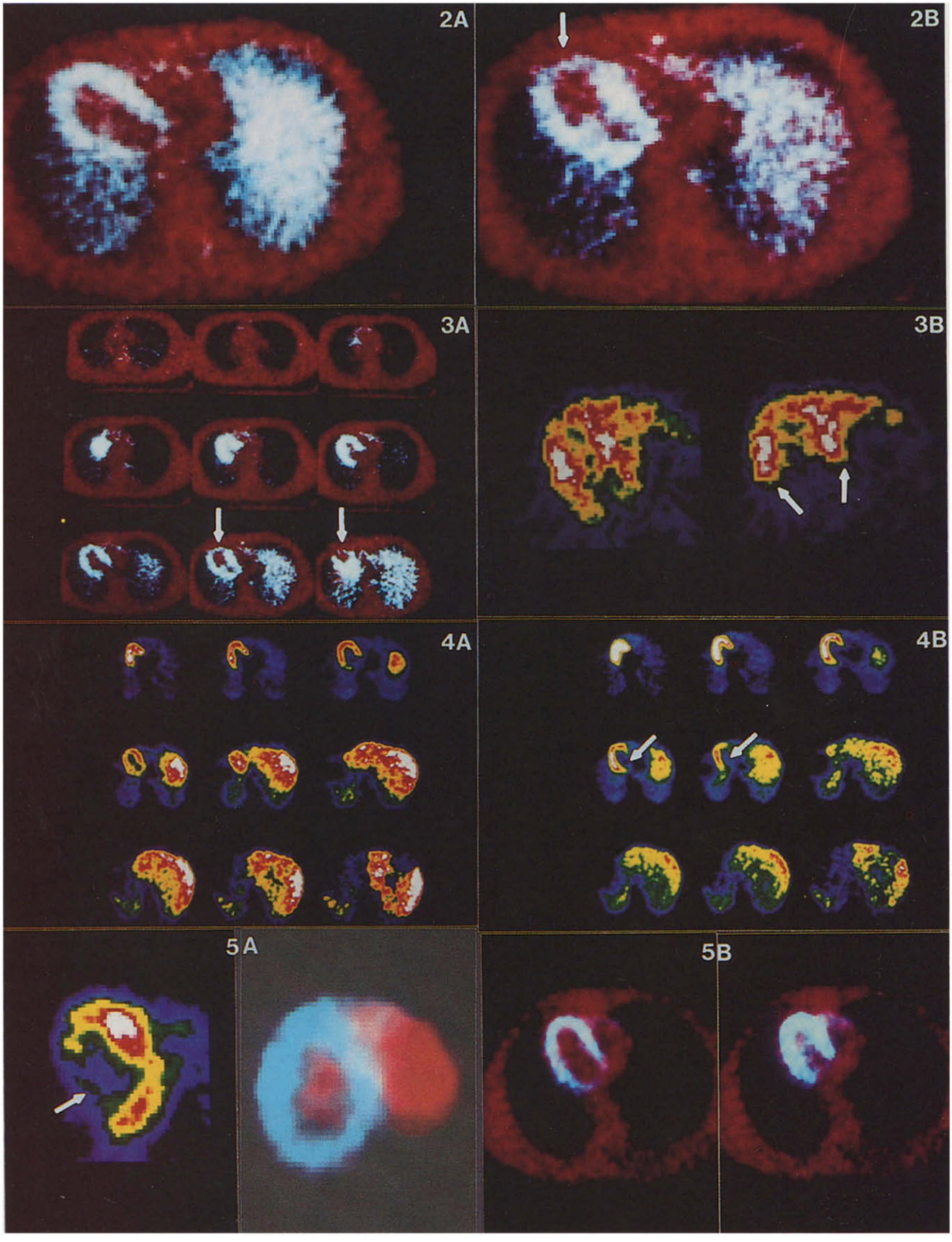

Figure 2. Single image plane after intravenous injection of $^{13}NH_3$ at rest (**A**) and after dipyridamole and handgrip (**B**). The red indicates the transmission image while the white indicates distribution of $^{13}NH_3$. The orientation is as if looking down on the heart from above with the apex of the left ventricle oriented superiorly, the left free wall on the left, the muscular septum on the right and the posterior wall inferiorly. The tomograph cuts the left ventricle along its longitudinal axis. **A**, Normal perfusion during conditions at rest; **B**, the comparable image after intravenous dipyridamole combined with handgrip stress. A large anterior wall defect (**arrow**) is apparent in which the counts are 50% below those of the normal area.

Figure 3. **A**, The nine simultaneous slices of this same patient after stress, oriented from the base of the heart on the **upper left** of the panel to the apex at the **lower right**. The first four image planes show no defect, whereas the most inferior two image planes demonstrate relative underperfusion (**arrows**). The stenosis is therefore in the mid left anterior descending coronary artery. **B**, A single image plane from another patient at rest (**left**) and with stress (**right**) in the isocount color format. With stress, there is a large lateral free wall and posterior septal defect (**arrows**) indicating both circumflex and right coronary artery disease.

Figure 4. **A**, Nine simultaneous slices in the isocount color format which is normal. **B**, These nine tomograms after stress with a large posterior defect (**arrows**).

Figure 5. **A**, Two images, the **leftmost** of which demonstrates a lateral defect (**arrow**) with stress, indicating single circumflex artery disease. The image at **right** demonstrates early phase/late phase imaging in which activity was collected for the first 60 seconds in red and after the first 60 seconds in blue. Thus, with a single intravenous injection of ^{82}Rb, both blood pool and perfusion images are obtained. **B**, Diastole (**left**) and systole (**right**) from gated tomograms in a normal patient.

coronary artery lesions and 9 right coronary artery lesions with an arteriographically determined coronary flow reserve of less than 3.0.

Figure 1A shows orthogonal arteriograms in left anterior oblique and right anterior oblique views before and after angioplasty as examples. Figure 1B shows the printout of an arteriographic analysis of these films before and after angioplasty. The data group in the upper left of the printout indicates identification, geometric dimensions of the stenosis and calibration factors; in the upper right is the graph predicting coronary flow reserve based on stenosis dimensions for this patient, as previously described (1); in the center left are pressure-gradient flow characteristics, in the center right are fluid dynamic coefficients dependent on geometry and at the bottom are reconstructions of the stenosis dimensions.

Positron imaging. Figure 2A shows a normal rest tomogram on the left with the transmission image in red and myocardial emission image in white with normal myocardial perfusion at rest. The image with dipyridamole-handgrip stress is shown in Figure 2B with a large anterior wall defect in which counts are 50% below the normal areas, indicating at least a 50% reduction in coronary flow reserve. In Figure 3A, the stenosis can be located to the mid-left anterior descending coronary artery because the top, or basal, four slices of the heart show no defect whereas the lower, or apical, two slices do show the defect. The coronary arteriogram for this patient shows a lesion in the mid-left anterior descending coronary artery (Fig. 1A). Quantitative analysis (Fig. 1B) had a 61% diameter narrowing in the left anterior oblique view, a 56% diameter narrowing in the right anterior oblique view, an area reduction of 83% narrowing and an arteriographically determined coronary flow reserve based on all stenosis dimensions of 2.4, or approximately 50% below normal, comparable with that found by positron imaging.

Figure 3B shows the normal rest (at left) and stress (at right) images with a large lateral and posterior defect. The isocount color format is shown. The two "horns" of the normal horseshoe shape are truncated on the stress image, indicating both left circumflex and right coronary disease and confirmed by coronary arteriography.

Figure 4A shows nine simultaneous slices from a patient at rest compared with Figure 4B, showing the stress image for this patient. These images were obtained with identical intensity and background settings. The nine slices sequenced from upper left to lower right correspond to progression from base to apex of the heart. Each set of nine slices is normalized to the peak counts in any one of the nine slices so that relative count intensity or color can be compared between slices as well as within a given slice. Normal tomographic anatomy has an open "C" shape progressively closing to a ring as the tomographic planes progress from base to apex. However, in this patient, there is no closing of the open "C" indicating a posterior defect corresponding to right coronary disease by arteriography.

Figure 5A (left image) shows the magnified stress images of a lateral defect corresponding to single left circumflex disease by arteriography. Figure 5A (right image) shows the diastolic blood pool (red) and perfusion images (blue) of a patient after a single intravenous injection of ^{82}Rb at rest. For this diastolic image the electrocardiographically gated count data were reconstructed from the first minute of data collection after intravenous injection of ^{82}Rb, shown as red. The data collected and reconstructed after the first minute after intravenous injection of ^{82}Rb are shown in blue-white. Thus, with a single intravenous injection, both blood pool (red) and perfusion images (white) can be obtained. The difference in integrated intensity of blood pool activity in the right ventricle and left ventricle, corrected for decay, can theoretically provide a measure of lung extraction of the tracer. The left ventricular blood pool activity on first pass of radionuclide also provides a direct measure of the arterial input function for calculating myocardial perfusion in absolute units of cubic centimeters per minute per gram according to the model previously reported from this lab-

JACC Vol 7, No 4
April 1986 775–89

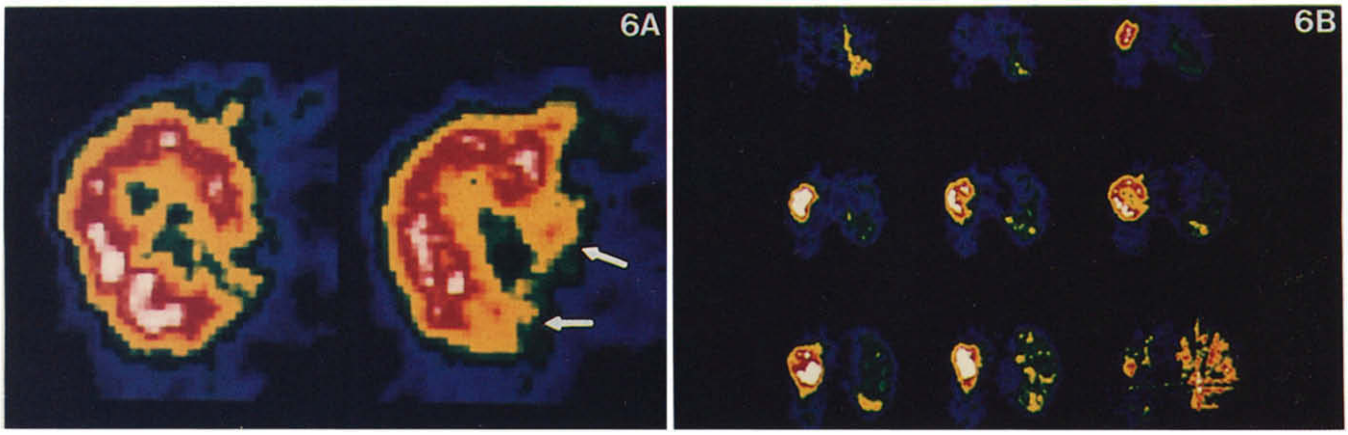

Figure 6. A, The rest-stress images from image plane 6 in the isocount color format. There appears to be a large posterior defect with stress (**arrows**). **B**, All nine slices of this same patient at rest with a normal anterior wall, the normal open "C" of the atrioventricular ring closing to a complete circle in the inferior slices.

oratory (22–24). Validation of the quantitative aspects of lung extraction and absolute perfusion measurement is a separate topic beyond the scope of this feasibility report. Figure 5B shows diastolic and systolic images of a normal patient with appropriate left ventricular wall thickening and systolic decrease in chamber size. It shows the transmission image in red and myocardium in white.

Translation of the heart images (changing patient position). Between the rest and stress images patients frequently moved despite vigorous efforts to maintain their position as well as referencing the mark on their chest to a fixed laser beam from the camera. With changing arm position, stretching or breathing, the skin may move over the chest wall causing a change of external landmarks in relation to the heart. Consequently, translation of the heart either vertically or laterally on the stress study as compared with the rest study was frequently observed. Figure 6A shows an example of this problem in comparing the rest (left) and stress (right) images from a fixed image plane, in this case, plane six. With stress there is an apparent large posterior defect, as might be observed with a single slice tomograph. However, Figure 7 is a schematic illustrating the problem of inferior translation of the patient between two studies, A and B. Consider study A to be at rest and study B to be with stress, but displaced inferiorly. A comparison of the rest-stress images in the same image plane outlined by the upper pair of dashed lines would suggest a large posterior stress defect. Similarly, if study B were the rest image and study A were the stress image displaced superiorly, then comparison of rest-stress images in the same image plane outlined by the lower dashed lines would suggest an anterior stress defect. However, by interpreting the entire set of images for the entire heart, the proper conclusions can be made.

The problem of slice displacement for Figure 6A can be seen in Figure 6B (rest) and Figure 8A (stress), showing all nine slices of each study in the isocount color format. In this case the first full slice of myocardium is seen on image plane three of the rest image but on image plane four of the stress image, indicating that the patient has moved

Figure 7. Schematic demonstrating the effect of image plane displacement on appearance of tomographs before (**A**) and after (**B**) an intervention. Single plane tomography or a multislice camera with undersampling between image planes will not allow identification of potential artifacts due to image plane displacement.

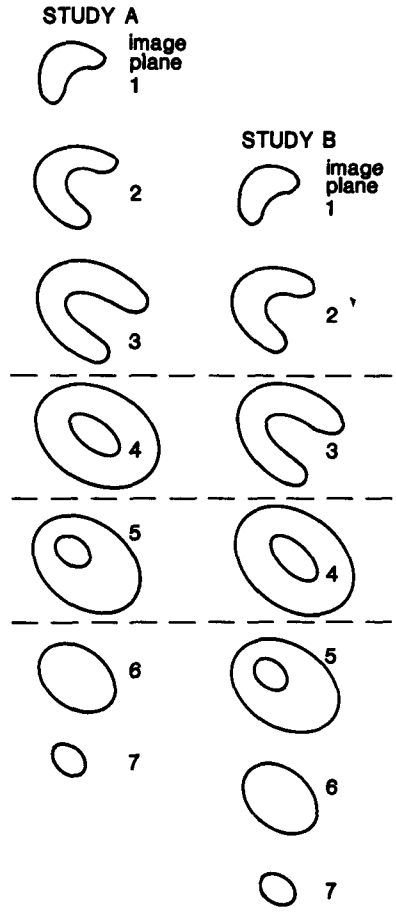

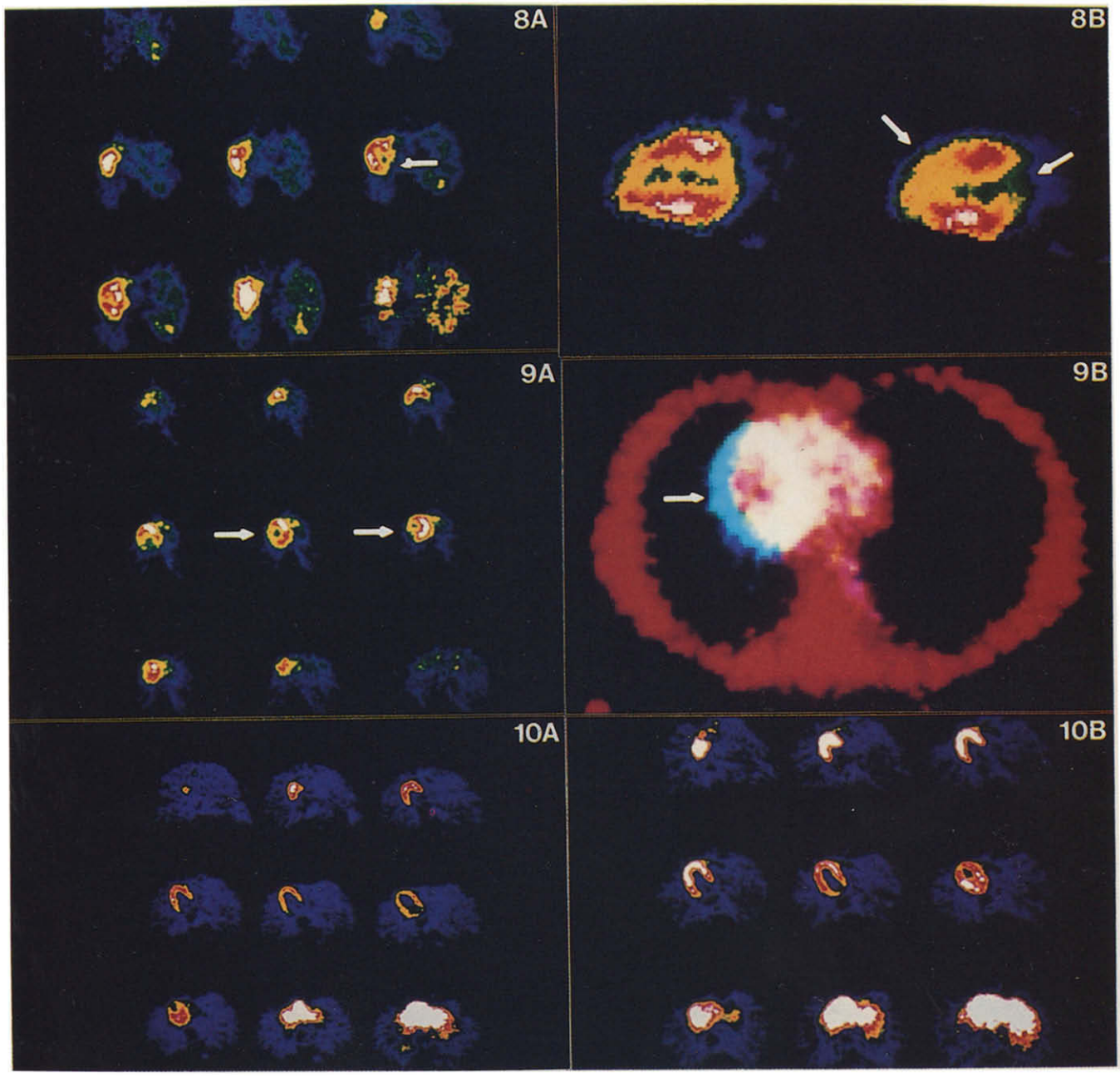

Figure 8. A, The nine slices of the same patient as in Figure 7 under stress. The patient moved inferiorly by one slice plane, such that the open "C" of the atrioventricular ring moved inferiorly, creating the impression of a posterior defect (**arrow**). **B**, The final correct answer on a longitudinal plane showing a small posterior stress defect (**right arrow**) and a slight decrease in relative anterior perfusion (**left arrow**) not seen on the horizontal slices.

Figure 9. A, the stress image of a patient with an apparent large, lateral perfusion defect (**arrows**). However, **B** shows the superimposition of the transmission (red) and emission (white) images for this patient. After the transmission scan, the patient moved to the left by approximately 1 to 2 cm such that the emission scan did not overlap the transmission scan. Accordingly, the attenuation correction is incorrect, thereby producing the appearance of a defect (**arow**).

Figure 10. A, Nine slices of a normal patient at rest; **B**, the stress images. The patient has moved superiorly between these two images, thereby giving the appearance of anterior apical thinning, which is due to slice displacement and not a coronary lesion.

inferiorly. Consequently, the apparent defect is due, in part, to that slice of myocardium, which brackets the open "C" pattern of the atrioventricular ring, moving inferiorly on the stress study. By interpreting the entire series of nine images, such displacement can be identified. A single slice tomograph or a multislice tomograph with gaps due to undersampling between image planes would therefore frequently

JACC Vol 7, No 4
April 1986:775–89

lead to erroneous interpretations. Senda et al. (25) also recently reported that image plane displacement may either cause apparent defects or obscure real defects on horizontal, skewed tomograms of the heart. For this reason, our camera has been designed for three-dimensional reconstruction with overlapping image plane to guarantee adequate sampling.

However, by reorienting the image planes in software, tomograms parallel to the long axis of the heart can be obtained in a left anterior oblique to right posterior oblique plane. The longitudinal tomograms in the left anterior oblique to right posterior oblique plane have the advantage of allowing comparison of the anterior and posterior myocardium in the same image without having to mentally translate color intensity comparisons between different images at different levels. Figure 8B shows these reoriented tomograms for the same patient illustrated in Figures 6A, 6B and 8A. The longitudinal slice clearly demonstrates a true posterior defect which, however, is not as large as that on the original horizontal tomograms where the defect has been exaggerated by slice displacement. The patient had a 46% diameter narrowing of the right coronary artery reducing the coronary flow reserve to 2.8 by automated quantitative arteriography. In addition, there is a failure to increase the activity in the anterior wall as much as the activity in the inferior lateral wall. This mild decrease in relative perfusion of the anterior wall is obvious on the longitudinal section but is not identifiable on the horizontal sections. It was associated with a 42% diameter narrowing of the left anterior descending artery, causing a modest reduction in coronary flow reserve to 3.7 by quantitative arteriography. Usually, an arteriographically determined coronary flow reserve of 3.7 is not associated with stress perfusion defects but on occasion can be seen, as in this case.

Figure 9A shows the effects of lateral translation. This stress image shows an apparent large lateral wall defect, identical to the rest image (not shown). Figure 9B shows the superimposition of the transmission image in red and the rest-stress images superimposed as white for this patient. The white rest-stress images are translated leftward from the transmission image by 1 to 2 cm because the patient moved after the transmission image was obtained. The apparent defect is then due to incorrect attenuation correction which becomes obvious if the three images—transmission, rest and stress—are superimposed on the tricolor presentation format. Therefore, we now use this format to check for displacement on images with apparent defects.

Figure 10A shows nine simultaneous slices of a normal patient at rest and Figure 10B shows those during combined dipyridamole-handgrip stress. Toward the apex, anterior thinning may normally occur while the posterior myocardial mass appears as a relatively greater area of activity. The final slices are below the left ventricular chamber appearing as a uniform circle of activity. The stress study is translated superiorly causing apparent apical thinning in slice six. Interpretation of all nine slices indicates this to be a normal study. With dipyridamole-handgrip stress, the relative myocardial to background ratio is visually much higher than at rest; it provides a visual qualitative indication of the patient's coronary vasodilatory response by comparison with the image at rest.

^{82}Rb versus ^{13}NH$_3$ images. The quality of images obtained with ^{82}Rb were comparable with those with ^{13}NH$_3$ for comparable total dose of activity reaching the myocardium. For example, Figures 2, 3A, 4, 5B and 10 were obtained after intravenous injection of 15 mCi of ^{13}NH$_3$. Figures 3B, 5A, 6, 8 and 9 were obtained after intravenous injection of 30 to 60 mCi of ^{82}Rb. Adequate images, but frequently of inferior quality, are obtained after injection of 30 mCi of ^{82}Rb (75 second half-life) because up to one-half of this activity decays during the time required for intravenous infusion and passage through the venous system and lungs before reaching the heart. Thus, the quality of the images is a function of the dose given to compensate for the greater decay of ^{82}Rb up to the time of data acquisition. From an applications viewpoint, the two radionuclides show little difference other than differences in half-life. However, ^{13}NH$_3$ images typically have greater activity in the liver than those with ^{82}Rb.

Sensitivity and specificity. Determining sensitivity and specificity of imaging for the diagnosis of coronary artery disease requires a standard as a reference. This standard has traditionally been percent diameter narrowing of coronary stenoses, usually estimated visually from coronary arteriograms. However, we have previously documented the necessity of accounting for all stenosis dimensions that affect

Figure 11. Correlation of arteriographically determined coronary flow reserve derived from all stenosis dimensions compared with percent diameter narrowing alone.

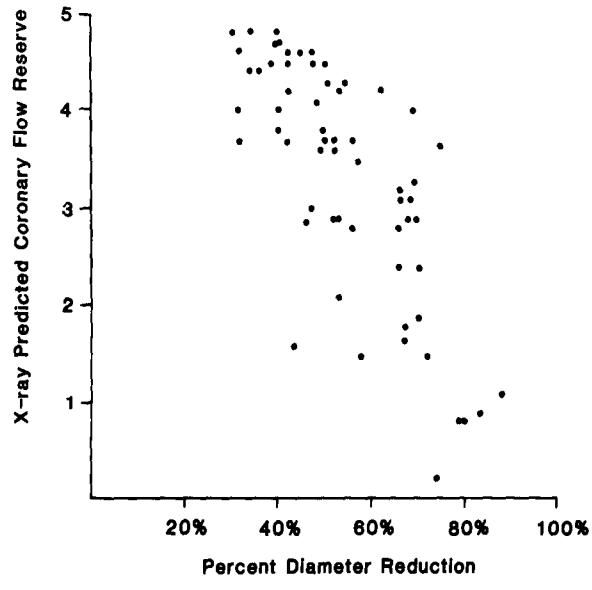

hemodynamic severity of stenoses (1,18,19), as confirmed by others (26,27). We have also previously documented in animals (1) that coronary flow reserve is a single, integrated measurement of severity, accounting for all stenosis dimensions of length, absolute diameter, relative percent narrowing and asymmetry. Furthermore, we have previously demonstrated in animals that percent diameter narrowing determined by X-ray film correlates poorly with flowmeter-measured coronary flow reserve and correlates poorly with arteriographically determined coronary flow reserve derived from all stenosis dimensions.

Consequently, for this study in patients, we needed to determine whether percent diameter narrowing was suitable as the reference standard for comparison with the perfusion images. We therefore compared arteriographically determined coronary flow reserve, as previously validated, with percent diameter narrowing for the 63 stenoses analyzed. The results are in Figure 11, showing a rough trend but with such great scatter that percent diameter narrowing was virtually useless as a reference standard. For example, a 60% diameter narrowing was associated with a range of arteriographically determined coronary flow reserve from 1.5 to 4.5, based on all stenosis dimensions. Because the perfusion defects seen on positron images during pharmacologic stress are related to coronary flow reserve, those defects would not be expected to relate to percent diameter narrowing. Therefore, we excluded the measurement of percent diameter narrowing alone as the reference standard for determining sensitivity and specificity of positron images for diagnosing coronary artery disease.

Figure 12 shows that percent area reduction correlated better with arteriographically determined coronary flow reserve based on all dimensions. An explanation for this better correlation is that most lesions are asymmetric and percent area reduction accounts for this asymmetry whereas percent diameter narrowing does not. However, there is considerable scatter about a steep curve such that for an individual stenosis, the percent area reduction is also unsatisfactory. For example, an 80% area reduction was associated with an arteriographically determined coronary flow reserve ranging from 2 to 4.5. Therefore, we also rejected area reduction alone as a reference standard.

Figure 12. Correlation of arteriographically determined coronary flow reserve derived from all stenosis dimensions compared with percent area reduction.

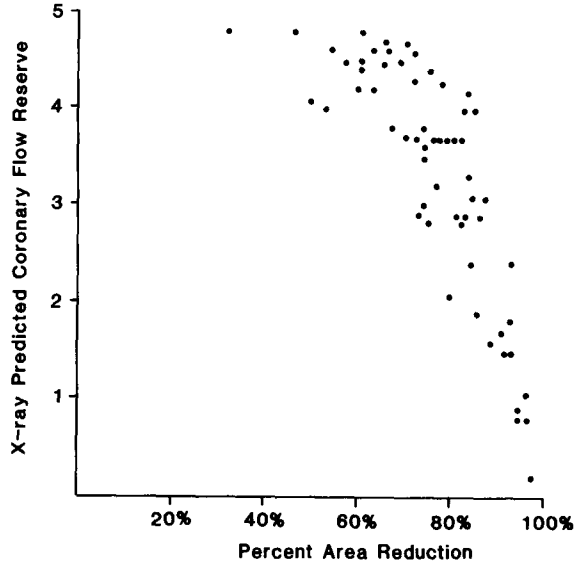

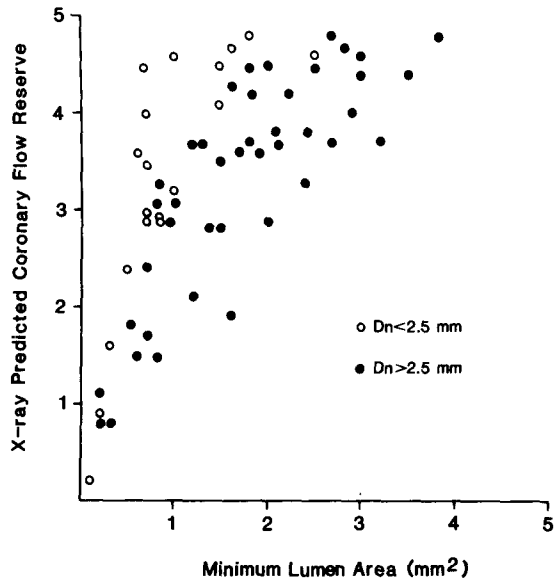

Figure 13. Correlation of arteriographically determined coronary flow reserve derived from all stenosis dimensions compared with minimal absolute cross-sectional area of stenosis for coronary arteries with normal diameter (Dn) less than (○) or greater than (●) 2.5 mm in diameter.

Minimal absolute cross-sectional lumen area of the stenosis has been previously suggested as a better measure of stenosis severity than percent narrowing (25,26). Accordingly, in Figure 13, we compared minimal absolute lumen area of the stenosis with arteriographically determined coronary flow reserve based on all stenosis dimensions. The correlation is poor because the effect of a given absolute minimal area will depend on the absolute diameter of the normal proximal artery and its length. A given stenosis cross-sectional area does not impair coronary flow reserve of a normally small vessel (<2.5 mm in diameter) but will reduce coronary flow reserve of a large artery (>2.5 mm normal proximal diameter). For example, an absolute minimal area of 1 mm^2 may be associated with a coronary flow reserve ranging from 1.5 to 4.5 depending on the diameter of the normal artery as well as the length of the stenosis. We therefore rejected absolute cross-sectional lumen area of the stenosis as a reference standard in this study.

Coronary flow reserve as the reference standard (<3 versus >3). As this and previous data (1) demonstrate, the only reference standard appropriate for comparison with

JACC Vol 7, No 4
April 1986:775–89

perfusion images is the arteriographically determined coronary flow reserve based on all stenosis dimensions of absolute diameter, relative percent narrowing, integrated length effects and asymmetry. Because the determination of sensitivity and specificity requires a binary "yes" or "no" interpretation of images, we chose, as the reference standard, to define significant coronary artery disease in these patients as an arteriographically determined coronary flow reserve of less than 3.0 in one or more main, proximal coronary arteries. We then determined the sensitivity and specificity of rest-stress positron imaging for identifying patients with an arteriographically determined coronary flow reserve of less than 3.0 in one or more major proximal coronary arteries.

The results of using the isocount color format described in the Methods section are shown in Table 1. Sensitivity was 95% in 22 patients with significant coronary artery disease defined as an arteriographically determined coronary flow reserve of less than 3.0. The one patient who was missed, studied with nitrogen-13 ammonia, had a 43% diameter narrowing of a ramus intermedius branch off the left coronary artery with no significant disease of the left anterior descending and left circumflex arteries. Specificity was 100% in nine patients without significant coronary artery disease as just defined.

The sensitivity and specificity of identifying significant coronary artery disease defined by the same arteriographic criteria but using the gray scale format and tricolor format for interpreting positron images are also shown in Table 1. These two formats for image interpretation relied on intensity of a gray scale or of a single color for identification of defects. Sensitivity using the gray scale format was 71% and by the tricolor format was 67%. The results are poorer because of the difficulty of interpreting intensity of a gray or unicolor scale and because of the problems of image plane displacement with slice by slice comparisons. The false negatives with the tricolor and gray scale formats involved different patients for three of the total of eight cases missed. Therefore, there was considerable unpredictability associated with these formats for interpreting images.

Thirteen patients had coronary artery disease but had an arteriographically determined coronary flow reserve equal to or greater than 3.0, that is, mild disease. The sensitivity of identifying these patients was 31, 38, and 31% by the isocount color, tricolor and gray scale formats, respectively.

Table 1. Sensitivity and Specificity for Identifying Patients With a Coronary Flow Reserve Less Than 3.0

	Format		
	Isocount Color	Tricolor	Gray Scale
Sensitivity	21 of 22 (95%)	67%	71%
Specificity	9 of 9 (100%)	100%	100%

Table 2. Sensitivity for Identifying the Coronary Artery With a Coronary Flow Reserve Less Than 3.0

Coronary Artery System	Sensitivity
Left (LAD, LCx, ramus intermedius)	16 of 18 (89%)
Right	9 of 9 (100%)

LAD = left anterior descending coronary artery; LCx = left circumflex coronary artery.

Thus, the limits of current sensitivity for diagnosing coronary artery disease is restricted to X-ray–determined flow reserve of less than 3. Although one-third of patients with milder disease were identified, the balance of those with milder disease were missed.

Left versus right coronary systems. Table 2 shows the sensitivity for identifying the artery involved in terms of either the left or right systems. With a highly variable distribution of location and size of the left anterior descending, left circumflex and ramus intermedius arteries, it was not possible to identify which subbranch was involved. The sensitivity for identifying the specific coronary artery with a flow reserve of less than 3.0 was 89% for the left and 100% for the right coronary artery. Of the two significant coronary lesions missed, one was a 43% diameter narrowing of a small ramus intermedius branch asociated with a coronary flow reserve of 1.6 in the previously described patient with no significant disease of the left anterior descending, left circumflex or right coronary artery. The other was a 68% diameter narrowing of a small ramus intermedius branch also, associated with a coronary flow reserve of 2.9 and insignificant disease of the left anterior descending and left circumflex coronary arteries but significant right coronary disease with a posterior defect. The latter patient also had poor counting statistics due to a suboptimal dose of ^{82}Rb. The values of percent diameter narrowing associated with an arteriographically determined coronary flow reserve of less than 3.0 ranged from 35 to 85% diameter narrowing (Fig. 11).

One patient with a perfusion defect was of particular interest. She had typical exertional angina pectoris, a positive thallium exercise test and a large anterior lateral defect on the positron image as well. However, this patient had a diminutive, diffusely small ramus intermedius branch without a localized stenosis supplying a large area of the anterolateral left ventricular wall, where the perfusion defect was observed.

Table 3. Side Effects of Intravenous Dipyridamole

Headache	46%	ST change	9%
Flushing	52%	Nausea	7%
Chest pain	24%	Dizziness	7%
Required aminophylline	13%	PVC; SVT	7%

PVC = premature ventricular complex; SVT = supraventricular tachycardia

Side effects of intravenous dipyridamole are shown in Table 3. Six patients had sufficient angina pectoris to require aminophylline for reversal, but no significant complications occurred.

Discussion

Relation of positron images to coronary arteriography. Positron emission tomography has been an esoteric, expensive research undertaking with little clinical utility to date. However, our results suggest that cardiac positron tomography using generator-produced ^{82}Rb can provide sensitive and specific diagnostic assessment of coronary flow reserve in humans utilizing a camera designed for imaging the entire heart and intravenous dipyridamole combined with handgrip stress. Tomographic image planes of the entire heart without gaps of undersampling between planes is essential to avoid errors in interpretation.

Our results also demonstrate that any single geometric measure of stenosis severity alone is an inadequate reference standard for comparison with perfusion images. The optimal reference standard is arteriographically determined coronary flow reserve derived from automated, quantitative analysis of *all* stenosis dimensions, including absolute normal and stenosis luminal area, percent narrowing, asymmetry and integrated length effects.

Arteriographically determined coronary flow reserve is theoretically and experimentally closely related to the relative distribution of a perfusion tracer in the heart during maximal coronary vasodilation. However, we emphasize that we have not measured coronary flow reserve directly by positron imaging. Rather, we have visually assessed relative perfusion defects under conditions of high coronary flow as a demonstration of clinical feasibility for noninvasively identifying coronary artery disease (28). Direct measurement of coronary flow reserve by positron imaging will require quantification of activity within a three-dimensional reconstruction of tracer distribution in the heart. Only then can the arteriographically determined coronary flow reserve be directly and systematically compared with that measured by positron imaging. However, three-dimensional quantification of activity and determination of absolute flow in cubic centimeters per minute per gram of myocardium has not yet been validated for imaging, although we have validated the basic model for such measurements using beta probes in animals (22–24).

Methodologic advantages and disadvantages. We are aware of the partial volume problems affecting every study of positron imaging published. However, because our camera has comparable resolution in the X, Y and Z axes, the partial volume problems are minimized compared with other cameras without these features. Despite these limitations to all positron imaging, our current study has demonstrated a major conceptual and practical step in the noninvasive assessment of coronary artery disease and an appropriate reference standard for the severity of stenoses not previously available.

^{82}Rb images are comparable in quality with those of $^{13}NH_3$ provided that an adequate dose is given, the optimum being 60 mCi, and no cyclotron is required. Other advantages of ^{82}Rb are that its half-life (75 seconds) is so short that data acquisition time is short, repeated sequential studies may be carried out, the radiation burden is low, push button operation by a single technician for emergency studies is feasible and, finally, the cost of each generator is fixed for a relatively unlimited number of studies by repeated elution. There was no difference in sensitivity and specificity between the two tracers in this small number of patients.

We have also demonstrated that with our camera, designed for high sensitivity and rapid imaging, ^{82}Rb can provide first pass gated blood pool images, as well as perfusion images by post-processing of data collected after a single intravenous injection of ^{82}Rb. From the blood pool images, the integrated arterial input function can theoretically be determined for calculation of absolute blood flow in units of cubic centimeters per minute per gram based on our previously described model (22–24). Finally, Goldstein (29) has previously demonstrated that viability of injured myocardium can be determined by following rubidium kinetics. Thus, positron imaging of generator-produced ^{82}Rb injected intravenously allows assessment of all the clinically essential characteristics of the heart: function, perfusion and viability. Cardiac positron tomography for clinical purposes has also become economically feasible because of the relatively inexpensive ^{82}Rb generator (Squibb) compared with a cyclotron and the decreased cost of positron cameras with our design.

For quantitative measurement of volumetric flow in cubic centimeters per minute per gram, the "speed" or sensitivity of the camera is important to quantify the first pass flow of tracer through the left ventricular cavity as the arterial input function for quantitative flow measurements (30). Our camera design is not a one of a kind instrument but is commercially available (Positron Corporation) with a positron camera now manufactured having two times the current sensitivity and twice the resolution, at a comparable or lower cost. Therefore, the remaining biologic problem for optimizing our approach is to develop still better stimuli for increasing coronary flow. It is reasonable to think that the optimal stress for an athletic 40 year old person would be different from that for an unsteady or ill 60 year old patient in whom sensitivity for early diagnosis of milder coronary disease is of less concern. For that reason, a spectrum of stimuli is needed involving different combinations of dipyridamole-exercise stress appropriate for a given type of patient and a given medical question to be asked. The usefulness of these further improvements in technique will be to identify still milder coronary artery disease more reliably

or to quantify the severity of coronary disease more accurately. Finally, as quantitation of myocardial perfusion is validated for clinical application, the conventional, binary, "all or nothing" classification of patients as having coronary disease or not, based on perfusion imaging, will have to be revised. Symptoms, prognosis, progression and therapy may have to be related to degrees of abnormalities in maximal perfusion for more physiologic and relevant medical decisions.

Conclusions. Our approach, begun 15 years ago, and now 30 years after the pioneering studies of Love and Burch (31), Mack et al. (32) and McHenry and Knoebel (33), is evolving rapidly toward an economically feasible, reliable screening test for symptomatic or asymptomatic coronary artery disease. Such an eventuality opens the opportunity for pharmacologic or mechanical interventions aimed at arresting or reversing coronary artery stenoses or preventing complications of myocardial ischemia or infarction in specific patients at an earlier stage than previously possible, thereby improving the chances of therapeutic success. However, larger numbers of patients and confirmatory studies are needed to define further the feasibility and economy of routine diagnostic positron imaging.

We are indebted to M. Matthews, RN, L. Parsel, RT, S. Adler, MS, J. Gaeta, MS, K. Yerian, MS, S. Marani, MS and M. Ranganath for their technical support of this project, to Kathryn Rainbird for coordinating the various parts of this project and to Claire Finn for manuscript preparation. Intravenous Persantine was kindly provided by Boehringer Ingelheim, Inc

References

1. Kirkeeide RL, Gould KL, Parsel L. Assessment of coronary stenoses by myocardial perfusion imaging during pharmacologic coronary vasodilation. VII. Validation of coronary flow reserve as a single integrated functional measure of stenosis severity reflecting all its geometric dimensions. J Am Coll Cardiol 1986;7:103–13.
2. Gould KL, Lipscomb K, Hamilton GW. Physiologic basis for assessing critical coronary stenosis. Am J Cardiol 1974;33:87–94.
3. Gould KL, Hamilton GW, Lipscomb K, Kennedy JW. A method for assessing stress induced regional malperfusion during coronary arteriography: experimental validation and clinical application. Am J Cardiol 1974;34:557–64.
4. Gould KL. Noninvasive assessment of coronary stenoses by myocardial imaging during coronary vasodilation. I. Physiologic principles and experimental validation. Am J Cardiol 1978;41:267–78.
5. Gould KL, Westcott JR, Hamilton GW. Noninvasive assessment of coronary stenoses by myocardial imaging during coronary vasodilation. II. Clinical methodology and feasibility. Am J Cardiol 1978;41:279–87.
6. Albro PC, Gould KL, Westcott RJ, Hamilton GW, Ritchie JL, Williams DL. Noninvasive assessment of coronary stenoses by myocardial imaging during pharmacologic coronary vasodilation. III. Clinical trial. Am J Cardiol 1978;42:751–60.
7. Gould KL. Assessment of coronary stenoses by myocardial perfusion imaging during pharmacologic coronary vasodilation. IV. Limits of stenosis detection by idealized, experimental, cross-sectional myocardial imaging. Am J Cardiol 1978;42:761–8.
8. Gould KL, Schelbert H, Phelps M, Hoffman E. Noninvasive assessment of coronary stenoses by myocardial perfusion imaging during pharmacologic coronary vasodilation. V. Detection of 47% diameter coronary stenosis with intravenous ^{13}NH and emission computed tomography in intact dogs. Am J Cardiol 1979;43:200–8.
9. Schelbert HR, Wisenberg G, Phelps ME, et al. Noninvasive assessment of coronary stenosis by myocardial imaging during pharmacologic coronary vasodilation. VI. Detection of coronary artery disease in man with intravenous $^{13}NH_3$ and positron computed tomography. Am J Cardiol 1982;49:1197–207.
10. Brown BG, Josephson MA, Peterson RB, et al. Intravenous dipyridamole combined with isometric handgrip for near maximal acute increase in coronary flow in patients with coronary artery disease. Am J Cardiol 1981;48:1077–85.
11. Yano Y, Budinger TF, Chiang G, et al. Evaluation and application of alumina-based ^{82}Rb generators charged with high levels of Sr-82/85. J Nucl Med 1979;20:961–6.
12. Mullani NA, Ficke DC, Hartz R, Markham J, Wong WH. System design of fast PET scanners utilizing time-of-flight. IEEE Trans Nucl Sci 1981;NS-28:104–8.
13. Philippe EA, Mullani N, Wong W, Hartz R. Real-time image reconstruction for time-of-flight positron emission tomography (TOFPET). IEEE Trans Nucl Sci 1982;NS-29:524–8
14. Mullani N, Wong W, Hartz R, Philippe E, Yerian K. Sensitivity improvement of TOFPET by the utilization of the interslice coincidences. IEEE Trans Nucl Sci 1982;NS-29:479–83.
15. Wong WH, Mullani NA, Phillipe EA, Hartz R, Gould KL. Image improvement and design optimization of the time-of-flight PET. J Nucl Med 1983;24:52–60.
16. Mullani NA, Gaeta J, Yerian K, et al. Dynamic imaging with high resolution time-of-flight PET camera—TOFPET I. IEEE Trans Nucl Sci 1984;NS-31:609–13.
17. Wong WH, Mullani NA, Wardworth G, Hartz RK, Bristow D. Characteristics of small barium fluoride (BaF_2) scintillator for high intrinsic resolution time-of-flight positron emission tomography. IEEE Trans Nucl Sci 1984;NS-31.381–6
18. Kirkeeide RL, Fung P, Smalling RW, Gould KL. Automated evaluation of vessel diameter from arteriograms. New York: Computers in Cardiology, Proceedings of IEEE Computer Society, 1982:215–8.
19. Kirkeeide RL, Smalling RW, Gould KL. Automated measurement of artery diameter from arteriograms (abstr). Circulation 1982;66(suppl II):II-325.
20. Gould KL, Kelley KO. Experimental validation of quantitative coronary arteriography for determining pressure-flow characteristics of coronary stenoses. Circulation 1982;66:930–7.
21. Gould KL, Kelley KO Significance of coronary flow velocity and changing stenosis geometry during coronary vasodilation in awake dogs. Circ Res 1982;50:695–704.
22. Mullani NA, Gould KL. First pass regional blood flow measurements with external detectors. J Nucl Med 1983;24:577–81.
23. Mullani NA, Goldstein RA, Gould KL, Fisher DJ, Marani SK, O'Brien HA. Myocardial perfusion with rubidium-82. I. Measurement of extraction fraction and flow with external detectors. J Nucl Med 1983;24:898–906.
24. Goldstein RA, Mullani NA, Fisher D, Marani S, Gould KL, O'Brien HA. Myocardial perfusion with rubidium-82. II. The effects of metabolic and pharmacologic interventions. J Nucl Med 1983;24:907–15.
25. Senda M, Yonebura Y, Tamaki N, et al. Axial resolution and the value of interpolating scan in multi-slice positron computed tomography (abstr). J Nucl Med 1985;26:11.
26. White CW, Wright CB, Doty DB, et al. Does visual interpretation of the coronary arteriogram predict the physiologic importance of a coronary stenosis? N Engl J Med 1984;310:819–24.
27. Harrison DG, White CW, Hiratzka LF, et al. The value of lesion cross-sectional area determined by quantitative coronary angiography in assessing the physiologic significance of proximal left anterior descending coronary arterial stenoses. Circulation 1984;69:1111–9.

28. Mullani NA. Myocardial perfusion with Rb-82. III Theory relating severity of coronary stenosis to perfusion defect. J Nucl Med 1984;25:1190–6.

29. Goldstein RA. Kinetics of Rb-82 after coronary occlusion and reperfusion. Assessment of patency and viability in open chest dogs. J Clin Invest 1985;75:1131–7.

30. Gould KL. Dynamic cardiac imaging. J Nucl Med 1984;25.1380–6.

31. Love WD, Burch GE. A study in dogs of methods suitable to estimating the rate of myocardial uptake of ^{86}Rb in man, and the effect of l-norepinephrine and pitressin on ^{86}Rb uptake. J Clin Invest 1957;36:468–78.

32. Mack RE, Nolting DD, Hogencamp CE, Bing RJ. Myocardial extraction of ^{86}Rb in the rabbit. Am J Physiol 1959;197:1175–7.

33. McHenry PL, Knoebel SB. Measurement of coronary blood flow by coincidence counting and bolus of ^{84}RbCl. J Appl Physiol 1967;22:495–500